A 400-GHz wideband high-gain quartz-based single-layered folded reflectarray antenna for terahertz applications

Miao, Zhuo-Wei; Hao, Zhang-Cheng; Wang, Yi; Jin, Biaobing; Wu, Jing-Bo; Hong, Wei

DOI:
10.1109/TTHZ.2018.2883215

Manuscript to be Published by the IEEE Transactions on Terahertz Science and Technology

A 400-GHz High-Gain Quartz-Based Single Layered Folded Reflectarray Antenna for Terahertz Applications

Zhuo-Wei Miao, *Student Member, IEEE*, Zhang-Cheng Hao, *Senior Member, IEEE*, Yi Wang, *Senior Member, IEEE*, Biao-Bing Jin, Jing-Bo Wu and Wei Hong, *Fellow, IEEE*

***Abstract*—Compact high-gain antennas are highly desired in the high speed terahertz (THz) wireless system, especially for the space limited application such as the high speed inter-link inside the high density wireless communication base station. To this end, a 400-GHz folded reflectarray (FRA) antenna with high gain, high aperture efficiency and compact profile is proposed in this paper. It is composed of a feed source, a single-layered reflectarray using a lithography process on quartz, and a wire-grid polarizer implemented by the printed-circuit-board (PCB) technology. A 3-D printed fixture is used to assemble all parts together. In order to design accurately the proposed antenna, the THz electromagnetic properties of the supporting dielectric materials are extracted by using a THz time-domain spectrometer system. Then, a single-layered phasing element, made up of a pair of orthogonally I-shaped structures with an open square ring, is proposed and designed based on the extracted material characteristics. Both phase compensation and polarization conversion can be realized by the proposed unit cell. A reflectarray is designed by using the proposed phasing element with the conventional array synthesizing theory, and a THz grid polarizer is designed with strips on a 0.127 mm Taconic TLY-5 substrate. The THz grid is placed in front of the THz feed and the reflectarray, which is fully reflective to the feed and transparent to the reflectarray. All components of the FRA antenna have been fabricated and assembled. Experiments show that the FRA prototype has a peak gain of 33.66 dBi at 400 GHz with an aperture efficiency of 33.65%, and a 3-dB gain bandwidth of 16% (357-421 GHz).**

***Index Terms*— Folded reflectarray antenna, terahertz, THz time-domain spectrometer, material characteristics, single-layer, quartz substrate, high-gain, 3-D printing.**

I. Introduction

TERAHERTZ (THz) technologies in the spectrum from 0.1 THz to 10 THz have been undergoing rapid development in recent years, and hold great potentials in applications such as biological detection [1], remote sensing [2], basic material research [3]-[5] and ultra-fast short-range wireless communications [6]-[7]. As a critical component to support the THz system, high-performance antennas are urgently required. A number of THz antennas have been reported over the past few years. These include horn antennas [8]-[10], reflector antennas [11]-[13], lens antennas [14]-[19] and cavity-backed slot antenna arrays [20]-[21].

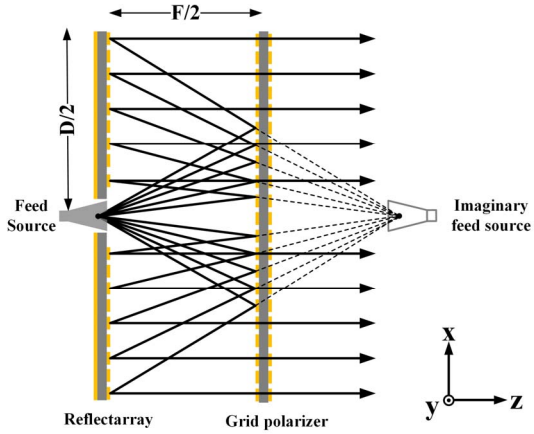

Fig. 1. Configuration of an FRA antenna.

Due to the limited power level of traditional wideband THz sources, high-gain antennas (over 30 dBi), such as reflector antennas, are of particular interest and in high demand. However, the traditional reflector antennas suffer from high manufacturing cost because of the high surface precision required in the fabrication process at submillimeter-wave and THz regions. As a competitive alternative to reflectors but with a more compact structure, significant advancement has long been made on planar reflectarray (RA) antennas, which combine the advantages of both reflector antennas and microstrip antenna arrays [22]. Driven by the demands of satellite communication, direct broadcasting services (DBS), and high-speed wireless communication, a variety of RA antennas have been developed and achieve expected radiation performances at microwave and low mm-wave frequency band [23]-[27]. When it comes to the THz frequency band, only a few reflective metasurfaces were demonstrated using the microfabrication techniques to manipulate THz waves [28]-[30]. In addition, transmitarray (TA) antennas, one kind of planar discrete lens but free from feeding blockage, would be

This work was supported in part by the National Natural Science Foundation of China No. 61471118, 61628104, and in part by the Scientific Research Foundation of Graduate School of Southeast University under Grant YBJJ1758. (*Corresponding Author* : Zhang-Cheng Hao)

Z.-W. Miao, Z.-C. Hao and W. Hong are with the State Key Laboratory of Millimeter-Waves, School of Information Science and Engineering, Southeast University, Nanjing 210096, China. (e-mail: zwmiao@seu.edu.cn, zchao@seu.edu.cn, weihong@seu.edu.cn)

B.-B. Jin and J.-B. Wu are with the Research Institute of Superconductor Electronics (RISE), School of Electronic Science and Engineering, Nanjing University, Nanjing 210093, China. (email: bbjin@nju.edu.cn)

Y. Wang is with the Department of Electronic, Electrical and Systems Engineering, University of Birmingham, B15 2TT, U.K. (email: Y.Wang.1@bham.ac.uk)

another promising choice to produce nearly arbitrary wavefront of electromagnetic waves. Some efforts have been made in TA antennas over 100 GHz, including beam collimation, beam focusing, beam deflection and polarization conversion [31]-[35].

To reduce the profile of the RA antennas further and avoid the feeding blockage, a more compact configuration, namely the folded reflectarray (FRA) antenna as shown in Fig. 1, has been proposed as a unique member of the RA family. This folded configuration is composed of a main reflectarray with an embedded feed source and a polarizing grid placed parallel to the RA with a distance h = F/2. The operation principle has been explained in [22] and is briefly described as follows. Linear-polarized spherical waves are generated by the feed source, whose electric fields are parallel to the strip grating. The electromagnetic waves are totally reflected back to the main RA by the polarizing grid. The main RA is designed to compensate the phase of the incident wave for beam shaping and to change the polarization by 90 degrees, so that the radiated waves can transmit through the polarizing grid. Finally, a pencil beam with high gain can be produced by the FRA antenna. Most of the existing FRA antennas are developed below 100 GHz using the commercial printed-circuit-board (PCB) technology or metallic milling process due to low manufacturing cost and ease of fabrication [36]-[41]. To expand the operating bandwidth, multilayered topologies are usually adopted in FRA designs [27], [41]. However, to our best knowledge, there is no experimental demonstration of high-performance THz FRA antennas in open literature. This is due to not only the difficulty of implementing multilayered topologies at THz region but also the limited performance of conventional single-layer phasing element. The latter is partly a result of limited information available about the dielectric properties of the substrates at THz frequency band.

In this paper, a low-cost single layered FRA antenna is proposed for THz wireless applications. It consists of a horn antenna as the feed source, a main reflectarray fabricated by lithography process on a quartz substrate, and a grid polarizer implemented by the PCB technology. A good radiation performance in gain, bandwidth and aperture efficiency will be demonstrated. Since the THz components are sensitive to the substrate characteristics such as the relative permittivity and loss tangent, which are not readily available from the manufacturer, the material parameters are first extracted by using the THz-TDS system. A single-layered phasing element with improved bandwidth and a grid polarizer are proposed and analyzed using the extracted material properties. A reflective unit cell, made up of a pair of orthogonal I-shaped structures surrounded by an open square ring, is employed in section II to manipulate independently the orthogonally polarized waves with sufficient phase coverage. To demonstrate the radiation performance, a 400-GHz FRA prototype with a circular aperture of 19.84 mm in diameter has been designed, fabricated and assembled in section III, together with detailed description of the THz measurement setup. Section IV presents measured results and discussions. Finally, conclusions are drawn in Section V.

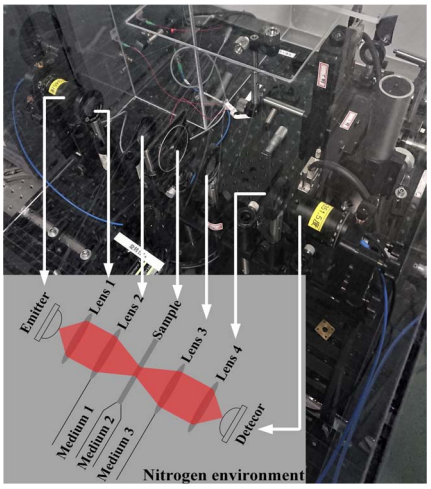

Fig. 2. Photography of the THz-TDS measurement system with corresponding schematic.

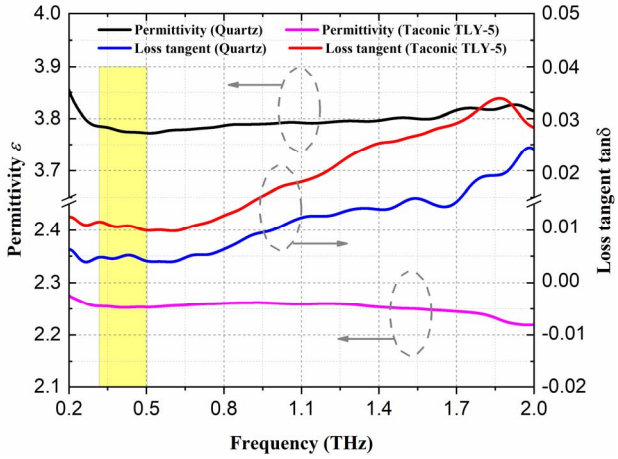

Fig. 3. The measured results of the relative permittivity and loss tangent.

TABLE I
EXTRACTED RESULTS OF THE MATERIAL PARAMETERS FOR DIFFERENT ESTIMATED THICKNESS OF THE SAMPLES AT 400 GHZ

Substrate	Thickness (mm)	Dielectric constant	Loss tangent
Quartz	1.005	3.780	4.428×10^{-3}
	1.006	3.776	4.445×10^{-3}
	1.007	3.773	4.462×10^{-3}
Taconic TLY-5	1.586	2.254	1.014×10^{-2}
	1.587	2.253	1.014×10^{-2}
	1.588	2.252	1.014×10^{-2}

II. ANALYSIS AND OPTIMIZATION OF THE REFLECTIVE ELEMENT AND GRID POLARIZER

The proposed FRA antenna is composed of a metallic feeding horn, a reflectarray and a grid polarizer. Different from the quartz substrates, whose THz electrical characteristics have been studied [5], there is very little information about the material properties of the Taconic TLY-5 substrates at THz region. Therefore, to ensure the accuracy of the FRA design, the extraction of the THz dielectric properties for both substrates should be carried out.

A. Extraction of the Dielectric Properties

Fig. 2 presents the THz-TDS system developed by Menlo Systems GmbH. The generated broadband THz beam is guided from the emitter to the samples via lens 1 and lens 2, for collimation and focusing, respectively. The spot diameter of the THz beam incident on the sample is about 3 mm. After transformation by lens 3 and lens 4, the beam is received by the detector. THz time-domain spectra of the samples are collected in transmission mode. The experiment is carried out in a glass dome filled with nitrogen at room temperature (about 300 K) and with a humidity level of less than 2%.

The extraction method proposed in [42] is used. A flat homogeneous sample is placed in the path of the THz radiation. To deal with the multiple reflections caused by the Fabry-Perot effect, the sample thickness is chosen to be sufficient large so as to ascertain the first directly transmitted THz pulse. The time-domain spectra of the air and solid sample are measured and transformed into frequency domain using fast Fourier transform. The amplitude $\rho(\omega)$ and phase $\varphi(\omega)$ of the complex transmission coefficient of the sample are obtained from the measured results. According to the equation (2) in [42], the values of $n(\omega)$ and $\kappa(\omega)$ can be extracted by using the Newton-Raphson method [4]. Finally, the dielectric constant ε and loss tangent tanδ can be calculated by the following equations

$$\varepsilon(\omega)=[n(\omega)-j\kappa(\omega)]^2 \tag{1}$$

$$\tan\delta=\varepsilon_i(\omega)/\varepsilon_r(\omega). \tag{2}$$

where $\varepsilon_i(\omega)$ represents the imaginary parts of the dielectric constant, and $\varepsilon_r(\omega)$ is the real part.

Fig. 3 presents the measured dielectric properties of the two substrates. The dielectric constant of the quartz decreases slowly from 3.785 to 3.773 as the frequency increases from 325 GHz to 500 GHz, while the loss tangent fluctuates within a small range from 3.66×10^{-3} to 4.77×10^{-3}. The Taconic TLY-5 substrate also has a stable relative permittivity of 2.253±0.001 within 325 to 500 GHz, while the loss tangent fluctuates within a small range from 9.43×10^{-3} to 1.11×10^{-2}.

The uncertainty of the extracted material parameters is also estimated here. It is worth pointing out that the accuracy depends mainly on the thickness of the sample [42]. In this experiment, one sample is a plate of quartz with a measured thickness of 1.006±0.001 mm, and the other is a plate of Taconic TLY-5 substrate with a measured thickness of 1.587±0.001 mm. Table I presents the extracted results of the material parameters for different estimated thickness of the samples at 400 GHz. The extracted relative permittivity and loss tangent change slightly with the thickness when the thickness error is about 0.001 mm, well within the acceptable range for the following FRA design. Several collimation lens are used in the experiment to reduce the divergence of the THz beam. It is also important to ensure that the THz beam impinges on the samples under test at a normal incidence.

B. Design of the Reflective Unit Cell

The detailed operation principle of the phasing element for the FRA antenna is presented in Fig. 4 (a). A linear polarized incidence with its electric field parallel to the grating is generated by the feed source, which would be reflected back to the main reflectarray with the same polarization. After the second reflection by the RA, the output field cannot pass through the polarizing grid if its polarization remains unchanged. Thus, the RA should be designed to produce a collimated wave and to implement the polarization rotation of 90º with respect to the polarization of incident electric field, so that the final radiated wave can be transmitted through the polarizing grid. In practical FRA designs, it is necessary to employ dual-polarized reflective phasing elements, and each unit cell in the RA should be rotated by 45º with respect to the polarization of incident electric field. Then, both the phase responses of the x-polarized and y-polarized reflective waves can be manipulated independently by adjusting the element sizes along x- and y- directions. It is worth pointing out that if

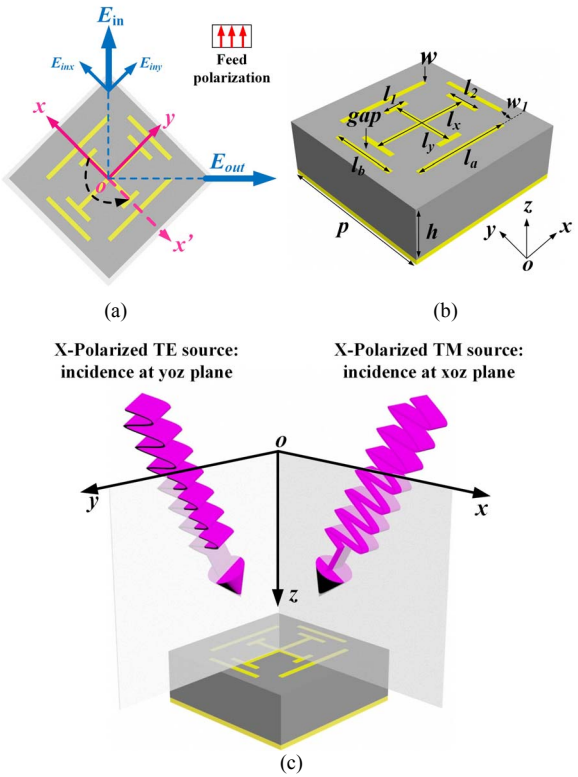

Fig. 4. (a) Schematic of the polarization rotation of the incident waves. (b) Geometry of the proposed reflective element. (c) Definition of the TE and TM source when the unit cell is excited by the x-polarized oblique incident plane wave.

TABLE II
GEOMETRICAL PARAMETERS OF Y-BAND PHASING ELEMENT

Parameters	Value (μm)	Parameters	Value (μm)
p	310	h	270
l_x	130 ~ 230	l_y	130 ~ 230
l_1	0.35×l_y	l_2	0.35× l_x
w	10	w_1	35
l_a	l_x-w	l_b	l_y-w
gap	20		

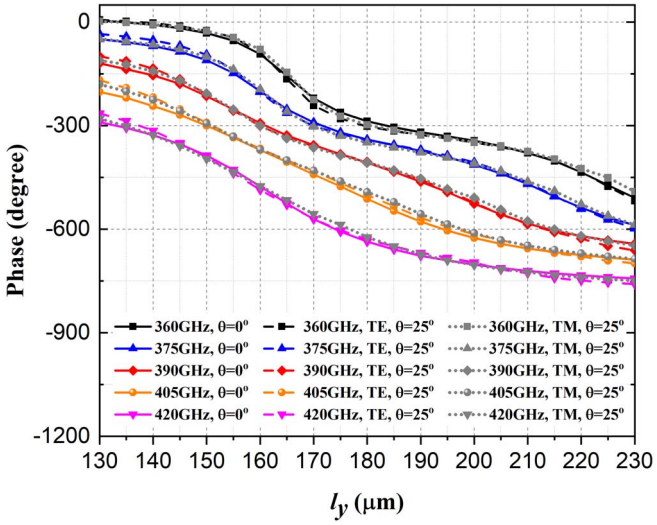

Fig. 5. Simulated phase responses of the reflective element under normal and 25° oblique y-polarized excitations at different frequencies when the parameter l_x is equal to 170 μm.

TABLE III
BRIEF SUMMARY OF THE SIMULATED REFLECTION COEFFICIENTS OF THE PHASING ELEMENT

	360 GHz		390 GHz		420 GHz	
	Mag (dB)	Phase change range (°)	Mag (dB)	Phase change range (°)	Mag (dB)	Phase change range (°)
Normal incidence	-0.94	>360	-0.92	>360	-0.84	>360
Oblique incidence (TE)	-0.91	>360	-0.99	>360	-1.38	>360
Oblique incidence (TM)	-0.84	>360	-0.93	>360	-1.80	>360

*The simulated magnitudes show in Table III are averaged.

an additional phase shift of 180º in the x-direction is provided by the unit cell, the radiated wave can pass through the grating because the polarization of the electric field are rotated by 90º. Considering the low cost and ease of fabrication at THz region, a single-layer reflective unit cell is preferred to the multilayered topology. Therefore, a dual-polarized single-layer reflective unit cell is designed here to manipulate independently the orthogonal polarized waves. The rectangular patch elements [40] and single Jerusalem cross elements [43] are the most popularly employed in the single-layer designs of dual-polarized unit cells. However, those unit cells are not able to provide adequate phase coverage (< 360 degrees), and suffer from nonlinear slope of the phase responses, which leads to a relatively low aperture efficiency and a narrow bandwidth [36]-[41].

As shown in Fig. 4(b), a multi-resonance reflective element is employed in this work to overcome the drawbacks of the conventional unit cells mentioned above. It is composed of a pair of orthogonally I-shaped structures surrounded by an open square ring. The mutual coupling between the two parts helps to enlarge the phase coverage and improves the linearity of the phase slope. The lengths of the I-shaped structures along x and y direction are denoted as l_x and l_y, respectively. The parameters l_1 and l_2 represent the lengths of load arms of the corresponding I-shaped structures. The size of the open square ring is controlled by the parameters l_a, l_b and w_1. The mutual coupling between the two parts, dominated by the parameter *gap*, is tuned carefully to obtain a desired linear phase response. In addition, to minimize the interference between the two orthogonal polarizations, the width of the center-connected part is chosen to be as small as possible within the machining precision. All the numerical verifications of the unit cell are performed using the full-wave simulation software FEKO with periodic boundary conditions (PBC) [44]. The detailed optimized geometry of the phasing element is summarized in Table II. In the simulation, the thickness of the quartz substrate is set as 270 μm, while the sputtering gold layer is 200-nm-thick. Based on the measured material properties, the relative permittivity ε_r and loss tangent tanδ of the quartz substrate at 400 GHz are set as 3.776 and 4.4×10^{-3} in the simulation. To adjust the reflective phase response with small steps, the unit cell periodicity is chosen to be 310 μm for achieving a high aperture efficiency in this work with a fine phase adjusting, which is $0.41\lambda_0$ at 400 GHz in free space. Both the x-polarized and y-polarized plane wave excitations need to be investigated for the unit cell. After parameter studies, the phase responses are found to be mainly dependent on the parameter l_y under y-polarized plane wave excitations, and the parameter l_x has little effect on the phase response. Similarly, when the unit cell is illuminated by an x-polarized plane wave, the phase responses are almost fully controlled by the parameter l_x rather than l_y. Therefore, the dual-polarized phasing element has the capacity to independently control the orthogonally polarized waves. It can be seen that the simulated phase responses under the orthogonally polarized waves are symmetric. In this work, only the reflective responses using a y-polarized plane wave are presented with a fixed parameter l_x of 170 μm.

Fig. 5 presents the simulated phase results of the reflective element under normal and 25-degree oblique y-polarized excitations at different frequencies. The simulated responses of the averaged magnitudes and phase are summarized in Table III. It can be seen that the phasing element covers over 360 degrees across the frequency band from 360 to 420 GHz by adjusting l_y from 130 μm to 230 μm under those two cases, and the unit cell has an averaged loss of less than 1 dB at normal excitations at 390 GHz. Since the focal length to diameter ratio (F/D) is chosen as 1.07 in this design, to be discussed in detail in section IV, the maximum angle of feed illumination is about 25 degrees. Then, the cases of oblique incidence including ($\theta = 25º$, $\varphi = 0º$) and ($\theta = 25º$, $\varphi = 90º$) are investigated with a TE or TM source, as defined in Fig. 4 (c). As shown in Fig. 5, the simulated phase responses indicate that the proposed unit cell is stable with acceptable phase variation. Hence, the proposed reflective unit cell is suitable for the design of FRA antennas.

C. *Design of the Grid Polarizer*

The THz grid polarizer in this work is fabricated using the PCB technology considering the fabrication cost and ease of implementation. A Taconic TLY-5 substrate with the thickness of 0.127 mm is employed in this design to support the parallel

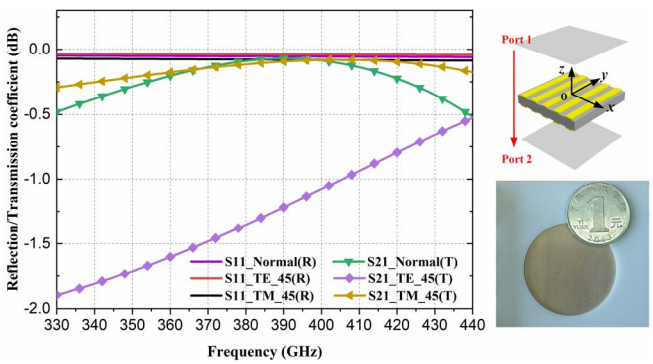

Fig. 6. Simulated responses of the grid polarizer using the PBC. ("R" represents the reflection mode under y-polarized excitation, and "T" represents the transmission mode under x-polarized excitation.)

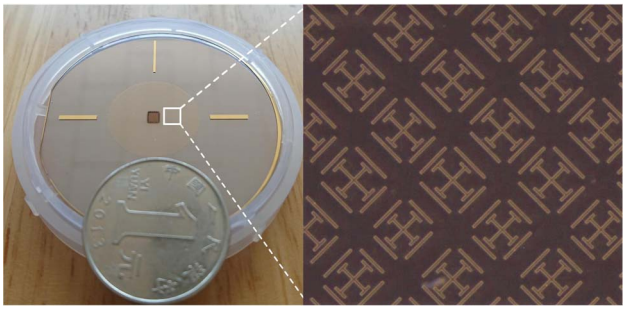

Fig. 7. Photograph of the fabricated reflectarray with its detailed structure.

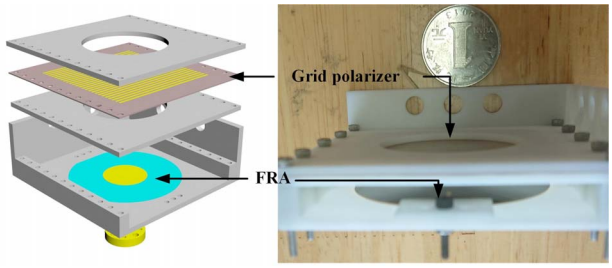

(a)

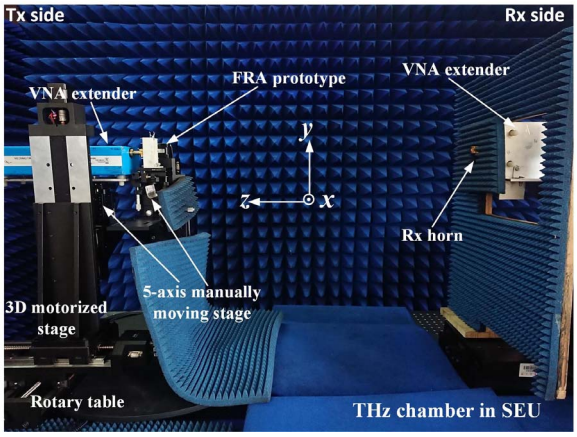

(b)

Fig. 8. (a) Assembly of the FRA antenna. (b) THz Measurement setup.

copper strips on both sides of the substrate. The measured relative permittivity and loss tangent of the substrate at 400 GHz are 2.2529 and 0.0101, respectively. Both the strip width and their separation are chosen as 0.1 mm, well within the

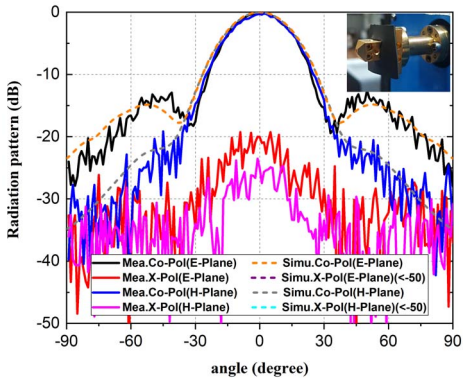

Fig. 9. Radiation patterns of the feed source at 400 GHz.

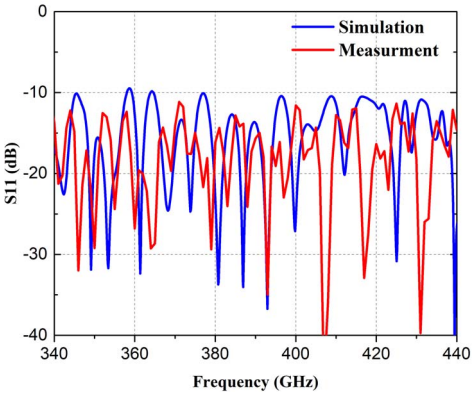

Fig. 10. Reflection coefficients of the THz FRA antenna.

machining precision. The conductivity of the copper layer is set as 5.8×10^7 S/m, and the thickness of the copper layer is 18 μm in this design. The copper layer occupies about half area of the grid polarizer, and its thickness cannot be ignored. The surface roughness of the copper layer should be taken into consideration, especially at the THz frequency band. The Hall-Huray theory, based on the stacked snowball model, is adopted in the simulation of the grid polarizer [45]-[47]. The surface of copper layer can be viewed as an irregular collection of nodules. The Hall-Huray model of the physical effects is causal, and can be characterized by two key parameters, nodule radius (NR) and surface ratio (SR). The parameter NR represents the radius of the copper sphere (snowball), and the parameter SR can be expressed as

$$SR = \frac{4\pi N \cdot NR^2}{A} \tag{3}$$

where the parameter N is the number of the snowballs in a unit cell, and A represents the area of the hexagonal geometry. In the simulation of the grid polarizer for the FRA design, the NR and SR are chosen as 0.5 μm and 3, respectively. The simulated S-parameters of the grid polarizer using the PBC is presented in Fig. 6, which shows that the y-polarized incident wave is almost fully reflected by the grid polarizer. The simulated transmission loss is less than 0.5 dB under x-polarized normal incidence.

Ideally, as a key component of the FRA antenna, the grid polarizer prototype needs to be tested and analyzed independently for the FRA design. However, it is difficult to extract accurately the transmission and reflection

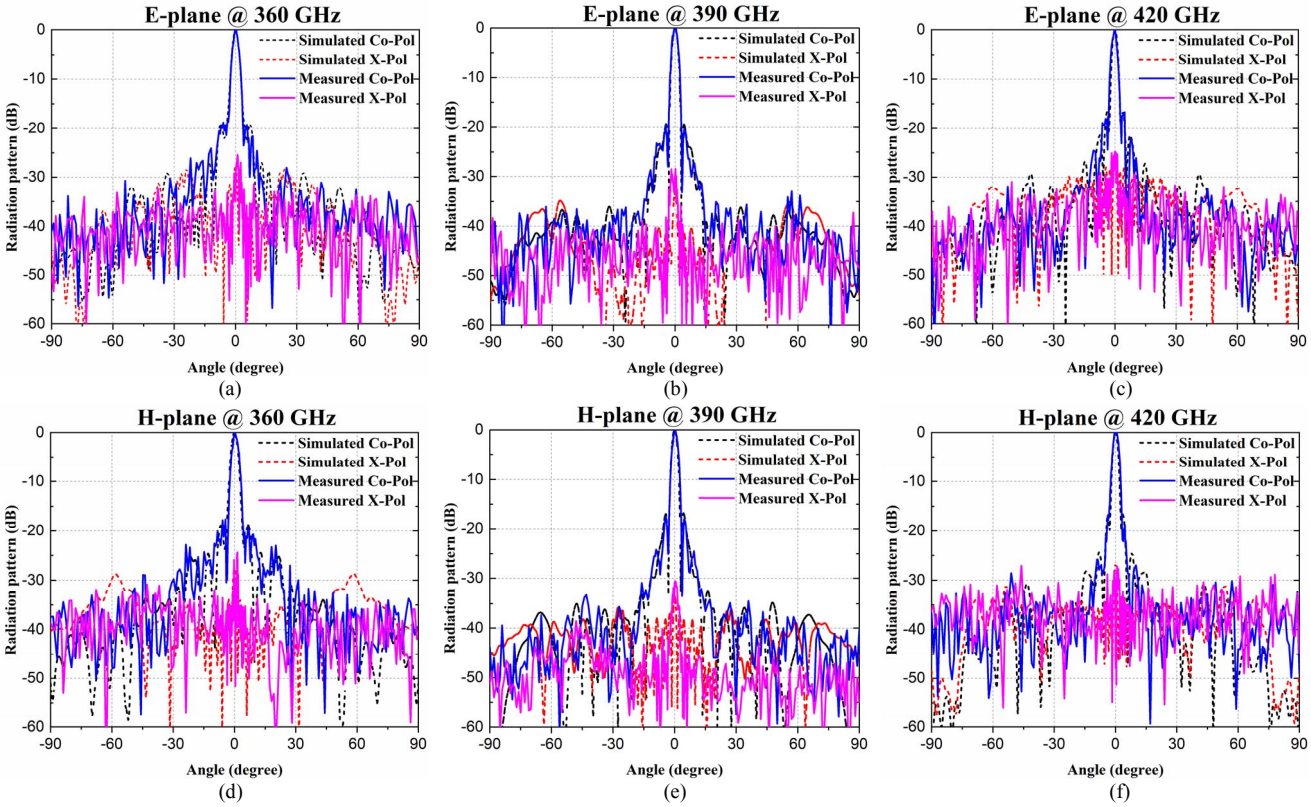

Fig. 11. Simulated and measured radiation patterns of the proposed THz FRA antenna.

TABLE IV
MEASURED RADIATION PERFORMANCE OF THE FRA ANTENNA

Frequency (GHz)	360		390		420	
	E-p	H-p	E-p	H-p	E-p	H-p
S.L.L (dB)	-18.8	-17.7	-20.5	-17.8	-16.7	-16.9
X-pol (dB)	-25.4	-24.1	-28.4	-30.6	-24.7	-27.9
HPBW (°)	2.9	3.0	2.5	2.5	2.4	2.3

TABLE V
TYPES OF THE DEFORMATIONS OF THE GRID POLARIZER

	Deformation type	**Mathematical expression**
Case I	Paraboloid	$x^2+y^2=2pz$
Case II	Paraboloid	$-(x^2+y^2)=2pz$
Case III	Parabolic cylinder	$x^2=2pz$
Case IV	Parabolic cylinder	$-x^2=2pz$
Case V	Parabolic cylinder	$y^2=2pz$
Case VI	Parabolic cylinder	$-y^2=2pz$

characteristics of the fabricated polarizer in the experiment due to multiple reasons: low output power and inadequate dynamic range of the THz OML frequency extender; small size of the fabricated polarizer; and the relatively low gain standard horn antennas used in the test setup. Nevertheless, we have used the Hall-Huray model to model the metal property and investigate the influence of the polarizer for the measured FRA in the following section, combined with the extracted dielectric property of the polarizer in Part A of section II.

III. FOLDED REFLECTARRAY PROTOTYPE AND THE THZ MEASUREMENT SETUP

Based on the ray tracing principle shown in Fig. 1, the required compensation phase of each element can be calculated using the following equation [22]:

$$\varphi_{mn} = k \times (r_{fmn} - \vec{u}_0 \cdot \vec{r}_{mn}) + 2\pi N, N = 0, \pm 1, \pm 2, \cdots \quad (4)$$

where r_{fmn} represents the distance between the imaginary feed source and the ***mn***th unit cell, u_0 denotes the unit vector, and r_{mn} represents the corresponding position vector. To verify the THz radiation performance, a reflectarray prototype is designed and fabricated using the lithography process. The reactive ion etching (RIE) technique, a type of dry etching, is adopted in the fabrication, and the used photoresist is AZ1350. We have used sputtering for the gold deposition to a thickness of 200 nm. The aperture of the main reflectarray, located at the center of a 2-inch wafer, is circular with a diameter D of 19.84 mm.

Since the substrate supporting the grid polarizer has a very thin thickness of 0.127 mm, deformation is not uncommon during assembling. If the grid polarizer is deformed, the radiation performance of the FRA antenna would be deteriorated because the ray traces are changed. As is shown in Fig. 8 (a), to effectively solve the problem, a set of support structures are manufactured by the 3-D printing technology. The grid polarizer can be placed exactly between the two square plates, and fixed accurately with the reflectarray embedded in the main supporter.

As shown in Fig. 8 (b), the experimental verification of the FRA antenna is performed in a THz anechoic chamber, using a vector network analyzer Agilent N5245A and a pair of OML WR 2.2 (325-500 GHz) waveguide extenders controlled by N5261A. After rough adjustment by the 3D motorized stage, it is necessary to employ two five-axis manually moving stages

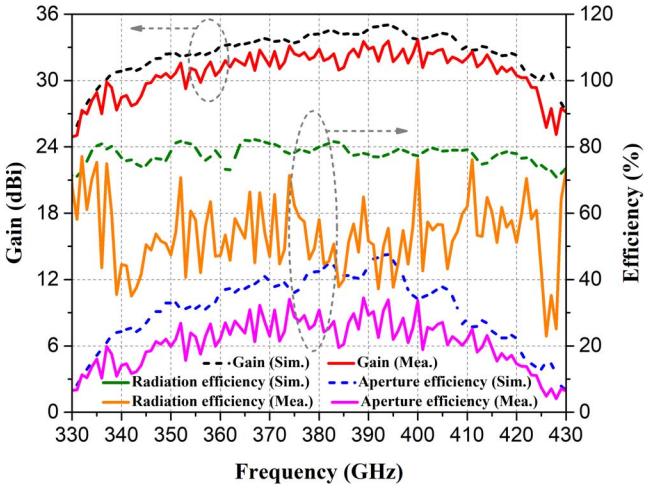

Fig. 12. Gain and corresponding efficiency of the proposed FRA.

(Zolix TSMW-XYZT-1) with the sensitivity of 3 μm for independent fine adjustments, which are installed under the assembled FRA prototype and the VNA extender at the TX side. The FRA antenna must be located at the rotation center of the electronic rotary table. Moreover, the IF bandwidth is set as 1 Hz in this experiment to maximize the signal-to-noise ratio.

IV. Measured Results and Discussion

A. Measured results of the Feed Source

The horn antenna is adopted as the feed source due to its stable radiation performance. A pyramid horn with a length of 2.2 mm is employed in this design with a rectangle aperture of 1.75×1.3125 mm^2. Fig. 9 presents the simulated and measured radiation patterns at 400 GHz, showing that the feed horn antenna has an equal flare angle of about 30º in the E-plane and H-plane. It should be mentioned that the degenerated cross polarization performance results from the small misalignment of the horn antennas and the weak multiple reflections between the horn antennas and the THz OML extenders. The pyramid horn obtains a wide operating bandwidth for $|S_{11}|$<-10 dB from 325 to 500 GHz. The measured half-power beamwidths (HPBW) in E-plane and H-plane are 27.79º and 27.02º, respectively. The measured gain of the horn is 16.14 dBi at 400 GHz. The F/D is chosen carefully to be 1.07 to provide a proper excitation, and the maximum oblique angle is about 25 degrees. According to the measured radiation performance, the minimum and maximum edge taper are -11.54 dB and -9.45 dB, respectively.

B. Measured Results of the THz FRA Antenna

The simulated and measured reflection coefficients of the assembled FRA antenna are compared in Fig. 10. Both are largely lower than -10 dB from 340 to 440 GHz.

After adjusting the positions of the feed horn and the assembled FRA prototype carefully by the manually moving stages, the radiation patterns in two principal planes are scanned by rotating the rotary table. Fig. 11 presents the measured and simulated radiation patterns at 360 GHz, 390 GHz and 420 GHz, all of which are normalized to their peak values. The detailed information about the side lobe level

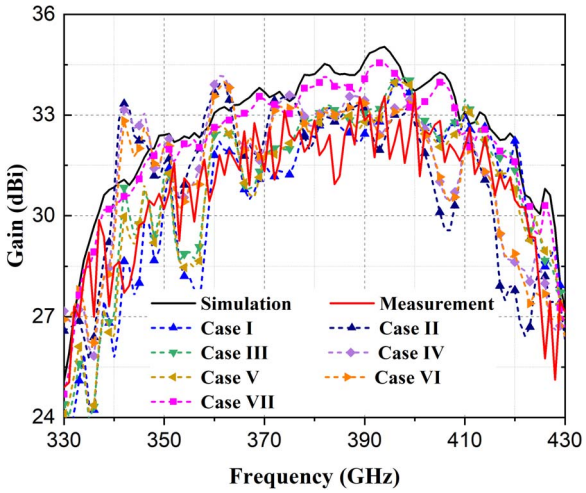

Fig. 13 Error analysis of the grid polarizer deformation and polarization mismatch. (Case I~VI: Grid polarizer deformations. Case VII: Polarization mismatch.)

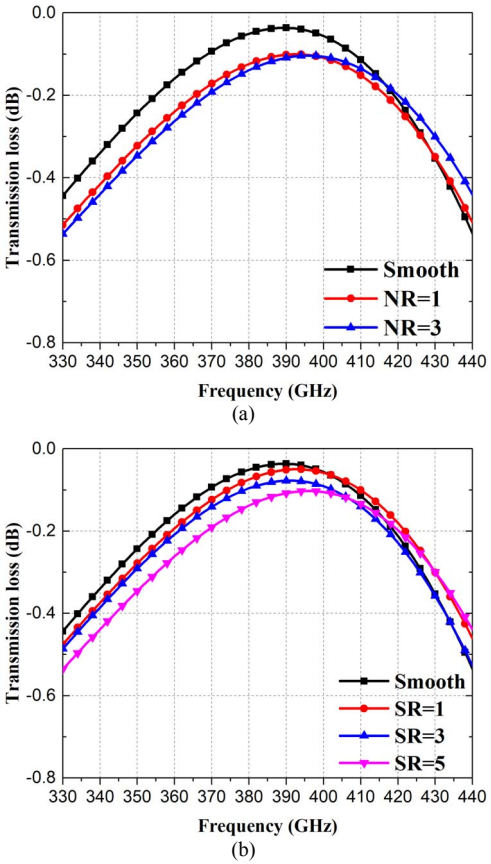

Fig. 14 Simulated transmission results of the grid polarizer with different setting of NR and SR under normal incidence.

(SLL), cross-polarization level (X-pol) and half-power beamwidth (HPBW) are provided in Table IV. Generally, the measured radiation patterns are well in agreement with the simulated results in the main radiation direction. According to the datasheet of the V02.2 VNA2 Series THz Vector Network Analyzer, the typical dynamic range of the measurement system is 55 dB. Since the received THz signal is very weak and the dynamic range is not adequately high, the differences of

the radiation patterns are mainly caused by the measurement errors.

As plotted in Fig. 12, by compared with a standard horn antenna provided by the VIVA TECH Corporation, the gain of the THz FRA antenna can be obtained. The measured 3-dB gain bandwidth is 357-421 GHz, and the maximum measured gain is 33.66 dBi at 400 GHz. The aperture efficiency η is defined using the following equation [21]:

$$\eta = \frac{G \cdot \lambda^2}{4\pi \cdot S_{FRA}} \tag{5}$$

where S_{FRA} represents the area of the THz FRA antenna. As shown in Fig. 12, the maximum measured aperture efficiency is 34.51% at 389 GHz.

C. Error Analysis and Discussion

The maximum gain difference of the FRA antenna between the simulated and measured results is about 3.33 dB in Fig. 12. The possible causes for the discrepancy include slight deformation of the grid polarizer, polarization mismatch and metal surface roughness of the grid polarizer. Full-wave simulations are performed to investigate those influences.

Firstly, despite of using the 3-D printed fixture for assembling, a slight deformation of the grid polarizer still cannot be avoided because of the relatively large aperture on a thin substrate. The grid polarizer cannot recover once it is deformed before the experiment.

To investigate the deformation, the shape of the grid polarizer can be modeled as paraboloids (2D deformation) or parabolic cylinders (1D deformation) shown in Table V. The corresponding coordinate is shown in Fig. 8. The ranges of the parameters are set as $|x|, |y| \leq 11$ mm. The parameter p is chosen as 242, which indicates that the distance between the apex of the paraboloid or the parabolic cylinder and the aperture surface is 0.25 mm, about a third of wavelength at 400 GHz in free space. The symbol "±" means that the paraboloids or parabolic cylinders are modeled along different directions. The types of the polarizer deformations are presented in Table V, and all the deformation cases are simulated. The simulated gain of the FRA antenna drops significantly when the grid polarizer is deformed. Secondly, the manual stage, shown in Fig. 8(b), is employed to realize five-axis fine adjustment, including the movement along x, y and z axes and the rotation around x and y axes. In the adjusting process, minor polarization mismatch between the feed source and the reflectarray is unavoidable. To show the effect of the polarization mismatch, the feed horn antenna is rotated by 3 degrees around z axis in the simulation. A gain reduction of about 0.5 dB can be observed in Fig. 13. Thirdly, the metal surface roughness of the grid polarizer should be taken into consideration as well. The Hall-Huray model mentioned above can be employed to analyze the surface roughness of the copper. The corresponding conductivity is set as 5.8×10^7 S/m. The simulated S-parameters of the grid polarizer with different combination of NR and SR using the PBC are presented in Fig. 14. Generally, it can be seen that the transmission loss of the grid polarizer increases with the parameters NR and SR, which also results in a slight reduction of the measured gain. In summary, the combined effects discussed above contribute to the discrepancies between simulated and measured results.

Table VI presents a comparison with some previous THz antennas, in terms of operating frequency, polarization, antenna dimensions, gain level, aperture efficiency, gain bandwidth, cross-polarization level and side lobe level. The proposed FRA antenna achieved a good radiation performance for THz application. In addition, according to the quotations from the manufacturers, a rough estimation of cost for each part has been

TABLE VI
COMPARISON WITH EXISTING WORKS ON THZ ANTENNAS

Reference	**This work**	[8]	[11]	[12]	[13]	[16]	[18]	[19]	[20]	[21]
Antenna type	**FRA**	Horn	Horn	Reflector	Reflector	Lens	Lens	Lens	Cavity-backed slot antenna	Cavity-backed slot antenna
Process	**Lithography + PCB**	Metallic milling	Metallic milling	SiC sintering	Metallic milling	LTCC	CNC milling	Metallic milling	MEMS (SiGe)	MEMS (Si)
Polarization	**LP**	LP	CP	LP	LP	LP	LP	LP	LP	LP
Center frequency f_0 (GHz)	**390**	1900	115	330	400	270	290	400	340	950
Aperture size (mm^2)	**309.15**	247	45.45	215448	88	167.42	452.39	9.68	1.21	1.08
Gain at f_0 (dBi)	**32.84**	-	18	55.3	28.5	20.8	29	24	7.9	14
Aperture efficiency at f_0	**29.29%**	-	~75%	~10.34%	~36.01%	~7%	~14.95	-	~31.57%	~18%
3-dB bandwidth (gain/AR)	**16%**	-	37%	-	37.5%	3.4%	30%	10%	5%	26.31%
X-pol level at f_0 (dB)	**-28.4**	-22	-17.5	-	-32	-45	-	< -30	-	-11
Side lobe level at f_0 (dB)	**-17.8**	-25	-20	-32	-9	-13	-9	-10	-	-10

Supplementary: (1) The radiation performances of the antennas are given by measured results. (2) The symbol "~" represents the calculated results which are not be provided directly.

TABLE VII
ROUGH ESTIMATION OF COST PER PIECE

Component	Process	Price ($)
Feed horn	Metallic milling	400
Reflectarray	Lithography	335
Polarizing grid	PCB	140
Assembly structure	3D-printing	15

listed in Table VII. Generally, the proposed antenna can be one of the promising low-cost candidates for high gain THz applications.

V. CONCLUSION

In this paper, a low-cost FRA antenna operating at THz frequency band has been proposed with high gain using hybrid fabrication technology. The reflectarray is fabricated on a quartz substrate, and a Taconic TLY-5 substrate is employed to support the parallel copper strips as the grid polarizer. The THz electrical characteristics of the two substrates are extracted using the THz-TDS measurement system. 3-D printed structures are adopted for stable assembling. To verify the proposed design, an FRA antenna prototype with a diameter of 19.84 mm has been fabricated and assembled. The measured gain of the FRA antenna is 33.66 dBi at 400 GHz with the corresponding aperture efficiency of 33.65%, and the 3-dB gain bandwidth is 357-421 GHz (16%).

ACKNOWLEDGEMENT

The authors would like to thank Q. Yuan, the State Key Laboratory of Millimeters, Southeast University, Nanjing, China, for his valuable discussions during the measurement.

REFERENCES

[1] K. B. Cooper, R. J. Dengler and N. Llombart et al., "THz Imaging Radar for Standoff Personnel Screening," *IEEE Trans. Terahertz Sci. Technol.*, vol. 1, no. 1, pp. 169-182, Sep. 2011. DOI:10.1109/TTHZ.2011.2159556.

[2] P. H. Siegel, "Terahertz Technology," *IEEE Trans. Microw. Theory Techn.*, vol. 50, no. 3, pp. 910-928, Mar. 2002. DOI:10.1109/22.989974.

[3] B. Ferguson and X. Zhang, "Materials for Terahertz Science and Technology," *Nature Mater.*, vol 1, pp. 26-33, 2002. DOI:10.1038/nmat708.

[4] L. Duvillare, F. Garet and J. Coutaz, "A Reliable Method for Extraction of Material Parameters in Terahertz Time-Domain Spectroscopy," *IEEE J. Sel. Areas Quant. Elec.*, vol. 2, no. 3, pp. 739-746, Sep. 1996. DOI:10.1109/2944.571775.

[5] M. Naftaly and R. E. Miles, "Terahertz time-domain spectroscopy for material characterization," *Proc. IEEE*, vol. 95, no. 8, pp. 1658-1665, Aug. 2007. DOI:10.1109/JPROC.2007.898835.

[6] H. Song and T. Nagatsuma, "Present and Future of Terahertz Communications" *IEEE Trans. Terahertz Sci. Technol.*, vol. 1, no. 1, pp. 256-263, Sep. 2011. DOI:10.1109/TTHZ.2011.2159552.

[7] M. Fitch and R. Osiander, "Terahertz Waves for Communications and Sensing", *John Hopkins APL Tech. Dig.*, vol. 25, no. 4, pp. 348-355, 2004. DOI:10.1142/S0218127404011569.

[8] N. Chahat, T. J. Reck and C. Jung-Kubiak et al., "1.9-THz Multiflare Angle Horn Optimization for Space Instruments," *IEEE Trans. Terahertz Sci. Technol.*, vol. 5, no. 6, pp. 914-921, Nov. 2015. DOI:10.1109/TTHZ.2015.2487781.

[9] P. Kittara, A. Jiralucksanawong and G. Yassin et al., "The Design of Potter Horns for THz Applications Using a Genetic Algorithm," *Int. J. Infrared and Millimeter Waves*, vol. 28, no. 12, pp.1103-1114, Dec. 2007. DOI:10.1007/s10762-007-9290-0.

[10] S. Bhardwaj and J. L. Volakis, "Hexagonal Waveguide based Circularly-Polarized Horn Antennas for Sub-mm-wave/Terahertz Band," *IEEE Trans. Antennas Propag.*, vol. 66, no. 7, pp. 3366-3374, Jul. 2018. DOI:10.1109/TAP.2018.2829842.

[11] N. Llombart, K B. Cooper and R. J. Dengler et al., "Confocal Ellipsoidal Reflector System for a Mechanically Scanned Active Terahertz Imager," *IEEE Trans. Antennas Propag.*, vol. 58, no. 6, pp. 1834-1841, Jun. 2010. DOI:10.1109/TAP.2010.2046860.

[12] H. Wang, X. Dong and M. Yi et al., "Terahertz High-Gain Offset Reflector Antennas Using SiC and CFRP Material," *IEEE Trans. Antennas Propag.*, vol. 65, no. 9, pp. 4443-4451, Sep. 2017. DOI:10.1109/TAP.2017.2724582.

[13] K. Fan, Z. Hao and Q. Yuan et al., "Development of a High Gain 325-500 GHz Antenna Using Quasi-Planar Reflectors," *IEEE Trans. Antennas Propag.*, vol. 65, no. 7, pp. 3384-3391, Jul. 2017. DOI:10.1109/TAP.2017.2705022.

[14] Q. Yu, J. Gu and Q. Yang et al., "All-Dielectric Meta-lens Designed for Photoconductive Terahertz Antennas," *IEEE Photonics Journal.*, vol. 9, no. 4, 5900609, Aug, 2017. DOI:10.1109/JPHOT.2017.2721503.

[15] F. Gaufillet, S. Marcellin and E. Akmansoy, "Dielectric Metamaterial-Based Gradient Index Lens in the Terahertz Frequency Range," *IEEE J. Sel. Areas Quant. Elec.*, vol. 23, no. 4, 4700605, Jul. 2017. DOI:10.1109/JSTQE.2016.2633825.

[16] J. Xu, Z. Chen and X. Qing, "270-GHz LTCC-Integrated High Gain Cavity-Backed Fresnel Zone Plate Lens Antenna," *IEEE Trans. Antennas Propag.*, vol. 61, no. 4, pp. 1679-1687, Apr. 2013. DOI:10.1109/TAP.2012.2232261.

[17] S. C. Saha, C. Li and Y. Ma et al., "Fabrication of Multilevel Silicon Diffractive Lens at Terahertz Frequency," *IEEE Trans. Terahertz Sci. Technol.*, vol. 3, no.4, pp. 479-485, Jul. 2013. DOI:10.1109/TTHZ.2013.2251929.

[18] K. Konstantinidis, A. P. Feresidis and C. C. Constantinou et al., "Low-THz Dielectric Lens Antenna With Integrated Waveguide Feed," *IEEE Trans. Terahertz Sci. Technol.*, vol. 7, no.5, pp. 572-581, Sep. 2017. DOI:10.1109/TTHZ.2017.2725487.

[19] Z. Hao, J. Wang and Q. Yuan et al., "Development of a Low-Cost THz Metallic Lens Antenna," *IEEE Antennas Wireless Propag. Lett.*, vol.16, pp.1751-1754, 2017. DOI:10.1109/LAWP.2017.2671880.

[20] X. Deng, Y. Li and W. Wu et al., "340-GHz SIW Cavity-Backed Magnetic Rectangular Slot Loop Antennas and Arrays in Silicon Technology," *IEEE Trans. Antennas Propag.*, vol. 63, no. 12, pp. 5272-5279, Dec. 2015. DOI:10.1109/TAP.2015.2490248.

[21] K. Luk, S. Zhou and Y. Li et al., "A Microfabricated Low-Profile Wideband Antenna Array for Terahertz Communications," *Sci. Rep.*, vol. 7, 1268, 2017. DOI:10.1038/s41598-017-01276-4.

[22] J. Huang and J. A. Encinar, Reflectarray Antennas. *IEEE Press*, John Wiley and Sons, Hoboken., 2008.

[23] R. Deng, S. Xu and F. Yang et al., "An FSS-Backed Ku/Ka Quad-Band Reflectarray Antenna for Satellite Communications," *IEEE Trans. Antennas Propag.*, vol. 66, no. 8, pp. 4353-4358, Aug. 2018. DOI:10.1109/TAP.2018.2835725.

[24] S. Montori, F. Cacciamani and R. V. Gatti et al., "A Transportable Reflectarray Antenna for Satellite Ku-band Emergency," *IEEE Trans. Antennas Propag.*, vol. 63, no. 4, pp. 1393-1407, Apr. 2015. DOI:10.1109/TAP.2015.2398128.

[25] J. A. Encinar, M. Arrebola and L. F. de la Fuente et al., "A Transmit-Receive Reflectarray Antenna for Direct Broadcast Satellite Applications," *IEEE Trans. Antennas Propag.*, vol. 59, no. 9, pp. 3255-3264, Sep. 2011. DOI:10.1109/TAP.2011.2161449.

[26] C. Tienda, J. A. Encinar and M. Arrebola, ""Contoured-Beam Dual-Reflectarray Antenna for DBS Application," *IEEE ISAP*, pp. 109-112, 3-8 Jul. 2011. DOI:10.1109/APS.2011.5996652.

[27] Z. Miao and Z. Hao, "A Wideband Reflectarray Antenna Using Substrate Integrated Coaxial True-Time Delay Lines for QLink-Pan Applications, " *IEEE Antennas Wireless Propag. Lett.*, vol.16, pp.2582-2585, 2017. DOI:10.1109/LAWP.2017.2734899.

[28] A. Tamminen, J. Ala-Laurinaho and S. Mäkelä et al., "Near-field measurements of submillimeter-wave reflectarrays," *Proc. SPIE*, vol. 8715, 871506, May. 2013. DOI:10.1117/12.2018606.

[29] T. Niu, W. Withayachumnankul and A. Upadhyay et al., "Terahertz Reflectarray as a Polarizing Beam Splitter," *Opt. Express*, vol. 22, no.13, pp. 16148-16160, Jun. 2014. DOI:10.1364/OE.22.016148.

[30] W. S. L. Lee, S. Nirantar and D. Headland et al., "Broadband Terahertz Circular-Polarization Beam Splitter," *Adv. Opt. Mater.*, vol. 6, no.3, 1700852, 2018. DOI:10.1002/adom.201700852.

[31] H. Yi, S. Qu and C. Chan, "Low-cost Two-layer Terahertz Transmit Array," *Electron. Lett.*, vol. 53, no. 12, pp. 789–791, Jun. 2016. (DOI: 10.1049/el.2017.1024.)

[32] Z. Miao, Z. Hao and G. Luo et al., "140 GHz High-Gain LTCC-Integrated Transmit-Array Antenna Using a Wideband SIW Aperture-Coupling Phase Delay Structure," *IEEE Trans. Antennas Propag.*, vol. 66, no. 1, pp. 182-190, Jan. 2018. DOI:10.1109/TAP.2017.2776345.

[33] C. Chang, D. Headland and D. Abbott et al., "Demonstration of a Highly Efficient Terahertz Flat Lens Employing Tri-Layer Metasurfaces," *Opt. Letters*, vol. 42, no.9, pp. 1876-1870, May. 2017. DOI:10.1364/OL.42.001867.

[34] X. Zhang, Z. Tian and W. Yue et al., "Broadband terahertz wave deflection based on C-shape complex metamaterials with phase discontinuities," *Adv. Mater.*, vol. 25, no.33, pp. 4567-4572, Jun. 2013. DOI:10.1002/adma.201204850.

[35] N. Grady, J. Heyes and D. Chowdhury et al., "Terahertz metamaterials for linear polarization conversion and anomalous refraction," *Science*, 1235399, May. 2013. DOI:10.1126/science.1235399.

[36] W. Menzel, D. Pilz and M. Al-Tikriti, "Millimeter-Wave Folded Reflector Antennas with High Gain, Low Loss, and Low Profile," *IEEE Trans. Antennas Propag.*, vol. 44, no. 3, pp. 34-29, Jun. 2002. DOI:10.1109/MAP.2002.1028731.

[37] W. Menzel, D. Pilz and R. Leberer, "A 77-GHz FM/CW Radar Front-End with a Low-Profile Low-Loss Printed Antenna," *IEEE Trans. Antennas Propag.*, vol. 47, no. 12, pp. 2237-2241, Dec. 1999. DOI:10.1109/22.808965.

[38] J. Zornoza, R. Leberer and J. A. Encinar et al., "Folded Multilayer Microstrip Reflectarray With Shaped Pattern," *IEEE Trans. Antennas Propag.*, vol.54, no.2, pp.510-518, Feb.2006. DOI:10.1109/TAP.2005.863101.

[39] A. Zeitler, J. Lanteri and C. Pichot et al., "Folded Reflectarrays with Shaped Beam Pattern for Foreign Object Debris Detection on Runways," *IEEE Trans. Antennas Propag.*, vol.58, no.9, pp.3065-3068, Sep.2010. DOI:10.1109/TAP.2010.2052564.

[40] J. Yang, Y. Shen and L. Wang et al., "2-D Scannable 40-GHz Folded Reflectarray Fed by SIW Slot Antenna in Single-Layered PCB," *IEEE Trans. Microw. Theory Techn.*, vol. 66, no. 6, pp. 910-928, Jun. 2018. DOI:10.1109/TMTT.2018.2818698.

[41] C. Zhang, Y. Wang and F. Zhu et al., "A Planar Integrated Folded Reflectarray Antenna With Circular Polarization," *IEEE Trans. Antennas Propag.*, vol. 65, no. 1, pp. 385-390, Jan. 2017. DOI:10.1109/TAP.2016.2623653.

[42] L. Duvillaret, F. Garet and J. Coutaz, "Highly precise determination of optical constants and sample thickness in terahertz time-domain spectroscopy," *Appl. Opt.*, vol. 38, no. 2, pp. 409-415, Jan. 1999. DOI:10.1364/AO.38.000409.

[43] H. Ma, G. Wang, G. Kong and T. Cui, "Independent Controls of Differently-Polarized Reflected Waves by Anisotropic Metasurfaces," *Sci. Rep.*, vol. 5, pp. 9605, 2015. DOI:10.1038/srep09605.

[44] HyperWorks FEKO 2017, Altair Engineering Inc., http://www.altairhyperworks.com/product/FEKO.

[45] P.G. Huray, S.G. Pytel and S.H. Hall et al., "Fundamentals of a 3-D "Snowball" Model for Surface Roughness Power Losses", *11th Annual IEEE SPI Proceedings*, pp. 13-16, May. 2007. DOI:10.1109/SPI.2007.4512227.

[46] S. Pytel, P. Huray and S. Hall et al., "Analysis of copper treatments and the effects on signal propagation," in *Proc. IEEE 58th Electron. Compon. Technol. Conf.*, pp. 1144-1149, May.2008. DOI:10.1109/ECTC.2008.4550120.

[47] S. Hall, S. Pytel and P.G. Huray et al., "MultiGHz, Causal Transmission Line Modeling Methodology with a Hemispherical Surface Roughness Approach", *IEEE Trans. Microw. Theory Techn.*, vol. 55, no. 12, pp. 2614-2624, Dec. 2007. DOI:10.1109/TMTT.2007.910076.

Zhuo-Wei Miao (S'16) received the B.S. degree in electronics and information engineering from Nanjing Normal University, Nanjing, China, in 2014. He is currently pursuing the Ph.D. degree in electrical engineering with Southeast University, Nanjing, China.

Mr. Miao was a recipient of National Scholarship for Doctoral Students in 2017. His current research interests include the design of metasurface-based passive components and reflectarray/transmitarray antennas at both millimeter-wave and terahertz frequency band.

Zhang-Cheng Hao (M'08-SM'15) received the B.S. degree in microwave engineering from XiDian University, Xi'an, China, in 1997, and the M.S. degree and Ph.D. degree in radio engineering from Southeast University, Nanjing, China, in 2002 and 2006, respectively. In 2006, he was a Postdoctoral Researcher with the Laboratory of Electronics and Systems for Telecommunications (LEST), École Nationale Supérieure des Télécommunications de Bretagne (ENSTB), Bretagne, France, where he was involved with developing millimeter-wave antennas. In 2007, he joined the Department of Electrical, Electronic and Computer Engineering, Heriot-Watt University, Edinburgh, U.K., as a Research Associate, where he was involved with developing multilayer integrated circuits and ultra-wide-band components. In 2011, he joined the School of Information Science and Engineering, Southeast University, Nanjing China as a professor. He holds 20 granted patents and has authored and coauthored over 170 referred journal and conference papers. His current research interests involve microwave and millimeter-wave systems, submillimeter-wave and terahertz components and passive circuits, including filters, antenna arrays, couplers and multiplexers.

Dr. Hao has served as the reviewer for many technique journals, including *IEEE Trans. On MTT, IEEE Trans. On AP, IEEE AWPL* and *IEEE MWCL*, and served as the guest editor for the *IEEE T-MTT Special-Issue on IWS2018*. He was the recipient of the Thousands of Young Talents presented by China government in 2011 and the High Level Innovative and Entrepreneurial Talent presented by Jiangsu Province, China in 2012.

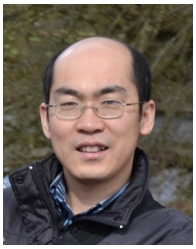

Yi Wang (M'09-SM'12) was born in Shandong, China. He received the B.Sc. degree in Physics and M.Sc. degree in Condensed Matter Physics from the University of Science and Technology, Beijing, China, in 1998 and 2001, respectively, and the Ph.D. degree in Electronic and Electrical Engineering from The University of Birmingham, Edgbaston, Birmingham, U.K., in 2005.

He started his career as a Research Fellow in 2004 at The University of Birmingham, working on high-frequency device applications of novel materials and structures. Between 2011 and 2017, he was a Senior Lecturer and Reader with University of Greenwich in the UK. He is now a Senior Lecturer with the University of Birmingham in the UK. His present research interests include multi-role microwave circuits and their co-design, antennas, micromachining, millimeter-wave and terahertz devices for metrology, communications and sensors. His minor interests are millimetre-wave measurements, and material characterizations.

Biaobing Jin received the Bachelor, Master and Ph. D. degrees in radio physics from Nanjing University, China, in 1986, 1991 and 1996, respectively. From 1995 to 1998, he was a lecture with Nanjing University of Post and Communication. He then received postdoctoral fellowship during Sept. 1998-July 2000 with National University of Singapore. From 2000 to 2004, he was a Visiting Scientist with the Institute of Thin Film and Interfaces, Research Center Juelich. From 2005 to 2006, he was awarded FWO fellowship with K. U. Leuven, Belgium. In November 2006, He became a full professor with Nanjing University. His research interests are superconducting electronics and THz devices.

Jingbo Wu received the B.S. degree in Electronic Information Science and Technology in 2005, the M.S. degree in Radio Physics in 2008, and the Ph.D. degree in Electromagnetic Field and Microwave Technology in 2012 from Nanjing University, China. He was a Radio Frequency Engineer in Huawei Company from 2008 to 2009. From 2012 to 2016, he was a Postdoctoral Researcher in University of Leeds and University of Cambridge, UK. From 2016, he joined School of Electronic Science and Engineering, Nanjing University and is an associate professor currently. His research interest includes terahertz metamaterials, plasmonics and spectroscopy.

Wei Hong (M'92-SM'07-F'12) received the B.S. degree from the University of Information Engineering, Zhengzhou, China, in 1982, and the M.S. and Ph.D degrees from Southeast University, Nanjing, China, in 1985 and 1988, respectively, all in radio engineering.

Since 1988, he has been with the State Key Laboratory of Millimeter Waves and serves for the director of the lab since 2003, and is currently a professor of the School of Information Science and Engineering, Southeast University. In 1993, 1995, 1996, 1997 and 1998, he was a short-term Visiting Scholar with the University of California at Berkeley and at Santa Cruz, respectively. He has been engaged in numerical methods for electromagnetic problems, millimeter wave theory and technology, antennas, RF technology for wireless communications etc. He has authored and co-authored over 300 technical publications with over 9000 citations, and authored two books. He twice awarded the National Natural Prizes, thrice awarded the first-class Science and Technology Progress Prizes issued by the Ministry of Education of China and Jiangsu Province Government etc. Besides, he also received the Foundations for China Distinguished Young Investigators and for "Innovation Group" issued by NSF of China.

Dr. Hong is a Fellow of IEEE, Fellow of CIE, the vice presidents of the CIE Microwave Society and Antenna Society, the Chair of the IEEE MTT-S/AP-S/EMC-S Joint Nanjing Chapter, and was an elected IEEE MTT-S AdCom Member during 2014-2016. He served as the Associate Editor of the IEEE Trans. on MTT from 2007 to 2010, one of the Guest editors for the 5G special issue of IEEE Trans. on AP in 2017.